**ICA-105574 interacts with a common binding site to elicit opposite effects on inactivation gating of EAG and ERG potassium channels**

Vivek Garg, Anna Stary-Weinzinger and Michael C. Sanguinetti

MOLECULAR PHARMACOLOGY

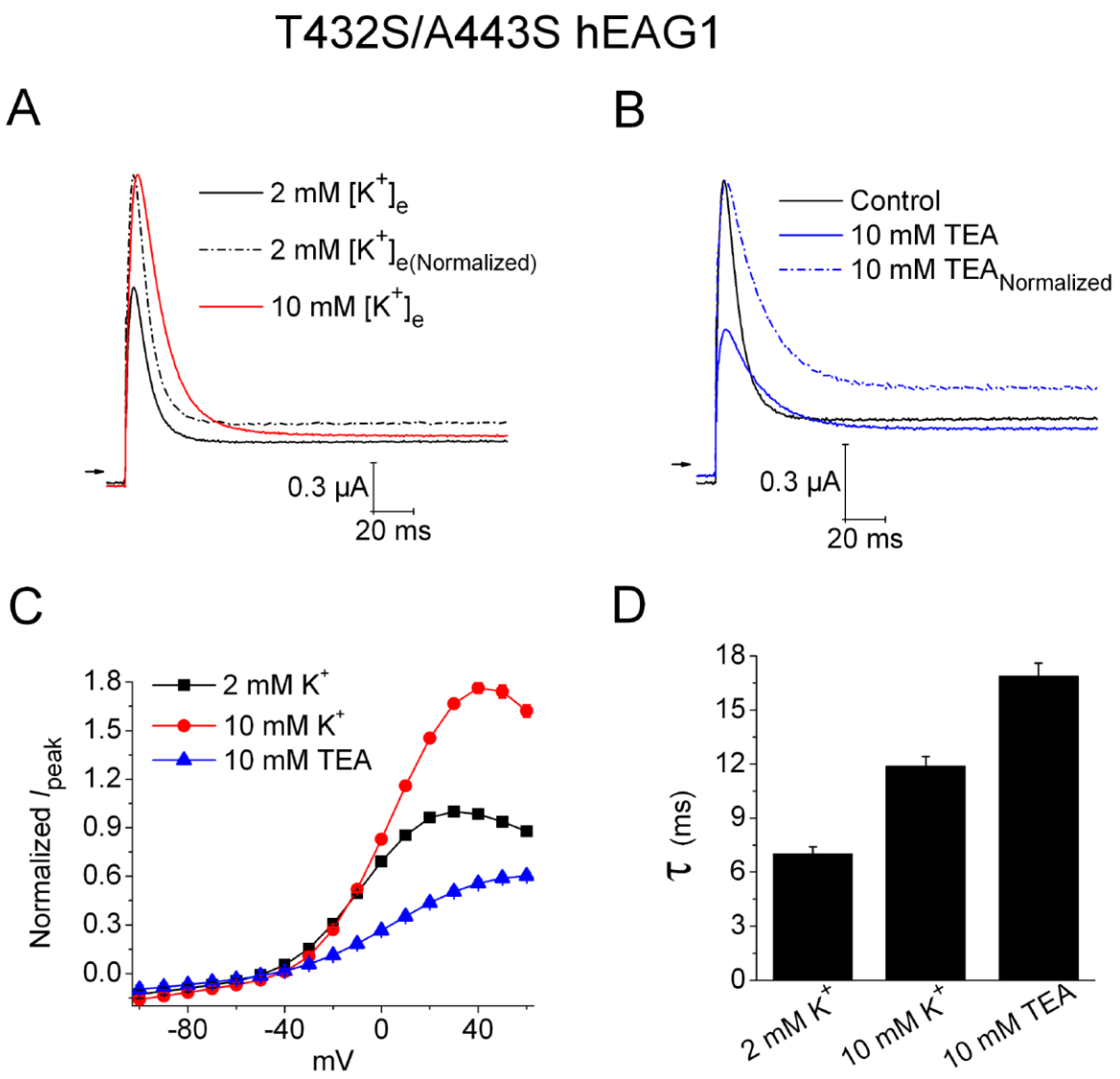


**Supplemental Fig. 1.** Elevated $[K^+]_e$ and extracellular tetraethylammonium (TEA, 10 mM) slow the rate of T432S/A443S hEAG1 inactivation. (*A*) Current elicited with a voltage step to +30 mV from a holding potential of –60 mV in the presence of extracellular solution that contained either 2 mM or 10 mM $[K^+]_e$. Dashed curve represents current measured with 2 mM $K^+$ scaled to match peak of current measured with 10 mM $K^+$. (*B*) Effect of 10 mM TEA on current from same oocyte shown in panel A**.** Dashed curve represents current measured with 10 mM TEA scaled to match peak of current measured under control conditions (2 mM $K^+$, no TEA). (*C*) Normalized $I_{peak}$-*V* relationships for T432S/A443S hEAG1 channels recorded under control conditions (2 mM $K^+$, ■) and in the presence of elevated $[K^+]_e$ (10 mM $K^+$, ●) and 10 mM TEA (▲) in the external solution ( *n* = 7). (*D*) Comparison of inactivation time constant (τ) at +30 mV in the presence of 2 mM $[K^+]_e$, 10 mM $[K^+]_e$ and 10 mM TEA (*n* = 7).

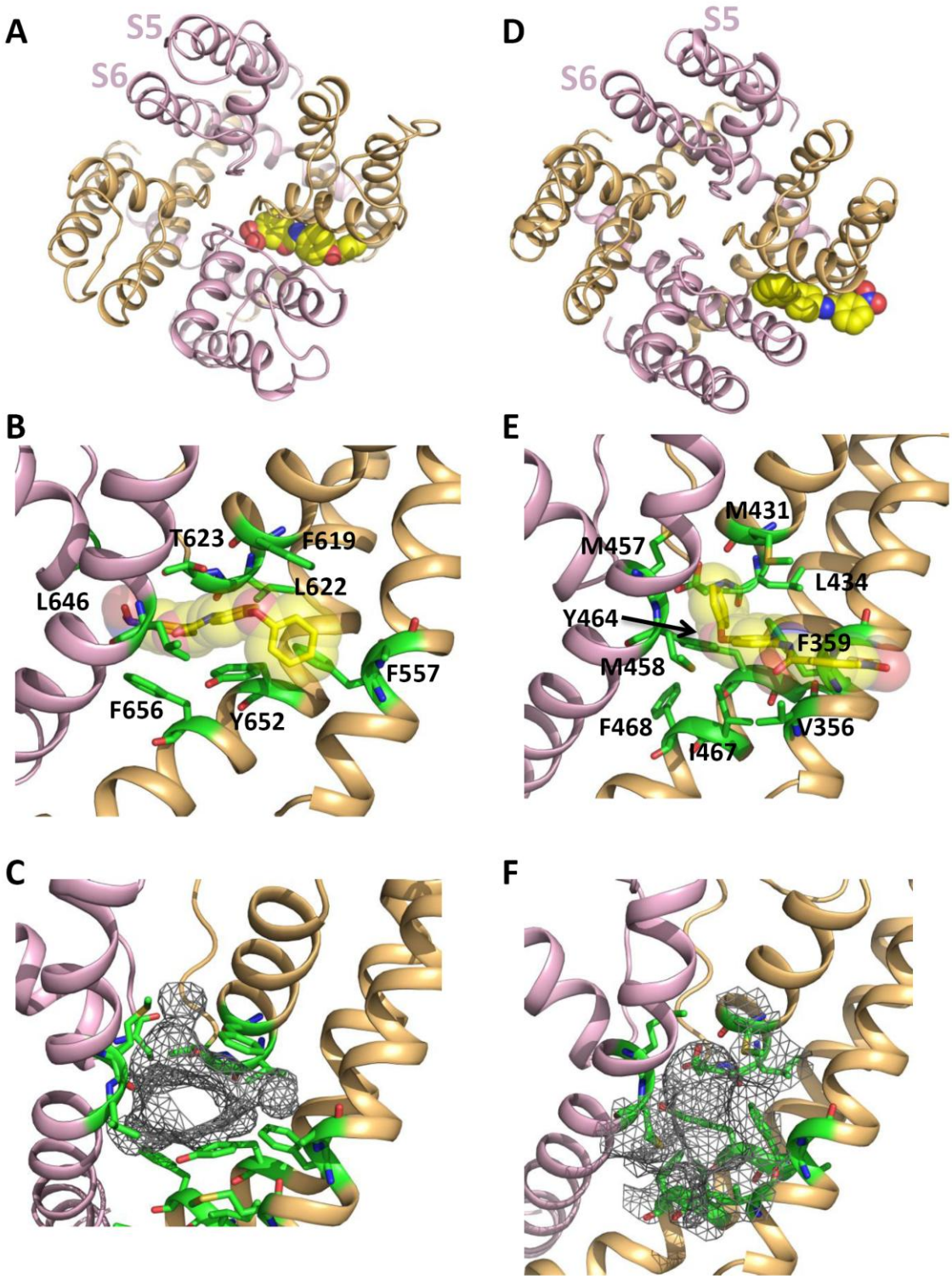


**Supplemental Fig. 2.** Comparison of simulated ICA dockings to homology models of hERG1 and hEAG1 pore modules in the open state. *A*, hERG1 pore module with ICA viewed from extracellular space. *B*, Side-view of ICA docked between two adjacent hERG1 subunits with interacting residues labeled. *C*, Map of ICA binding pocket located between two adjacent subunits of hERG1. *D*, hEAG1 pore module with ICA viewed from extracellular space. *E*, Side-view of ICA docked between two adjacent hEAG1 subunits with interacting residues labeled. *F*, Map of ICA binding pocket located between two adjacent subunits of hEAG1.

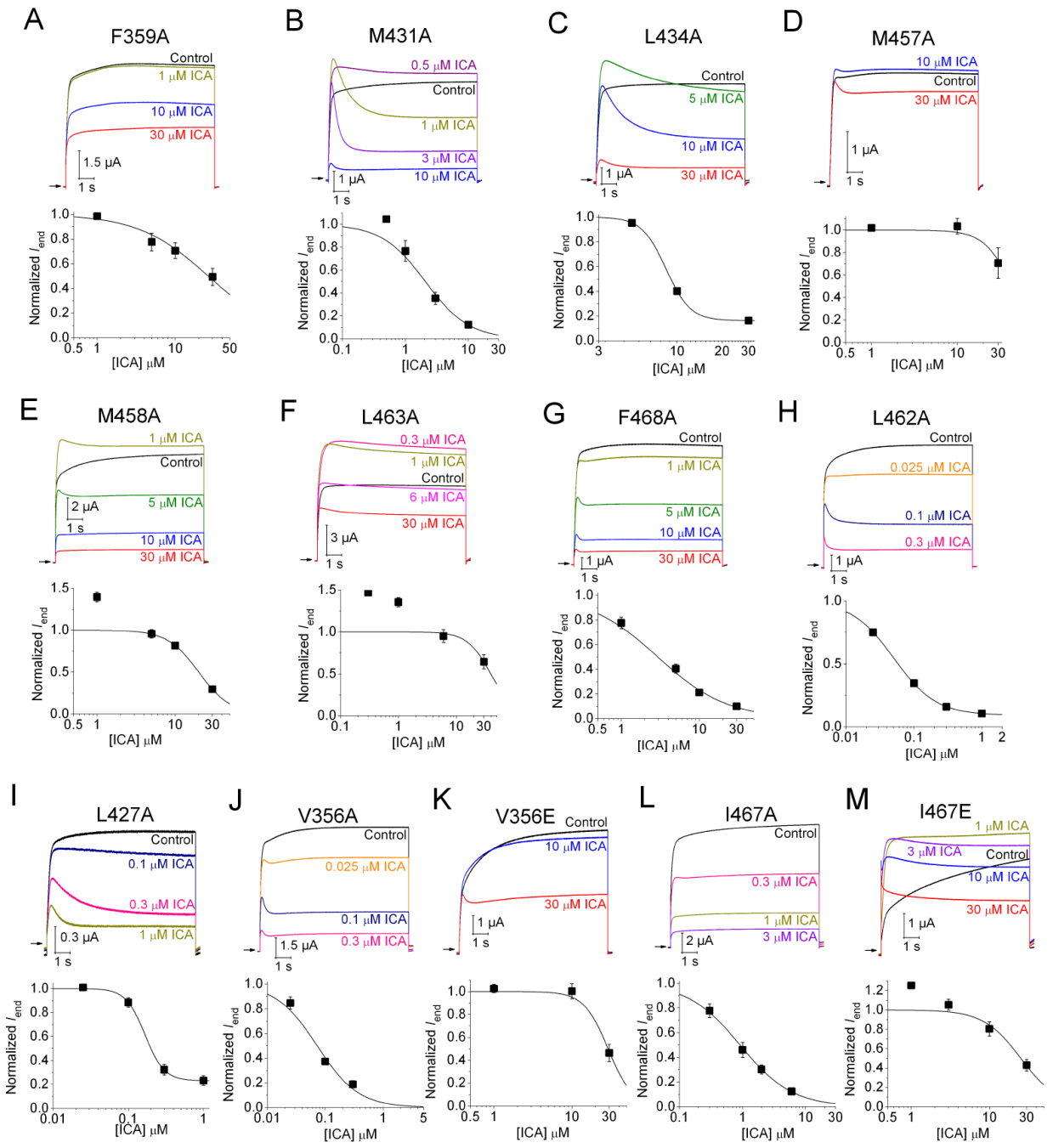


**Supplemental Fig. 3.** Effect of ICA on mutant hEAG1 channels. *A – L*, The 11 residues predicted by modeling to be in close proximity to ICA in either the open and closed state were mutated as indicated and the effect of ICA at the indicated concentrations on currents was measured. In each panel upper traces show currents measured during 10-s pulses to +30 mV. The [ICA]-response relationship for each mutant channel is plotted below each set of current traces. Leu427A, Met431 and Leu434 are located in the pore helix. Val356 and Phe359 are located in S5. Leu463, Ile467, Phe468 are located in S6 of one subunit, and Met457, Met458 and Leu462 are located in the S6 of an adjacent subunit (see Fig. 3).

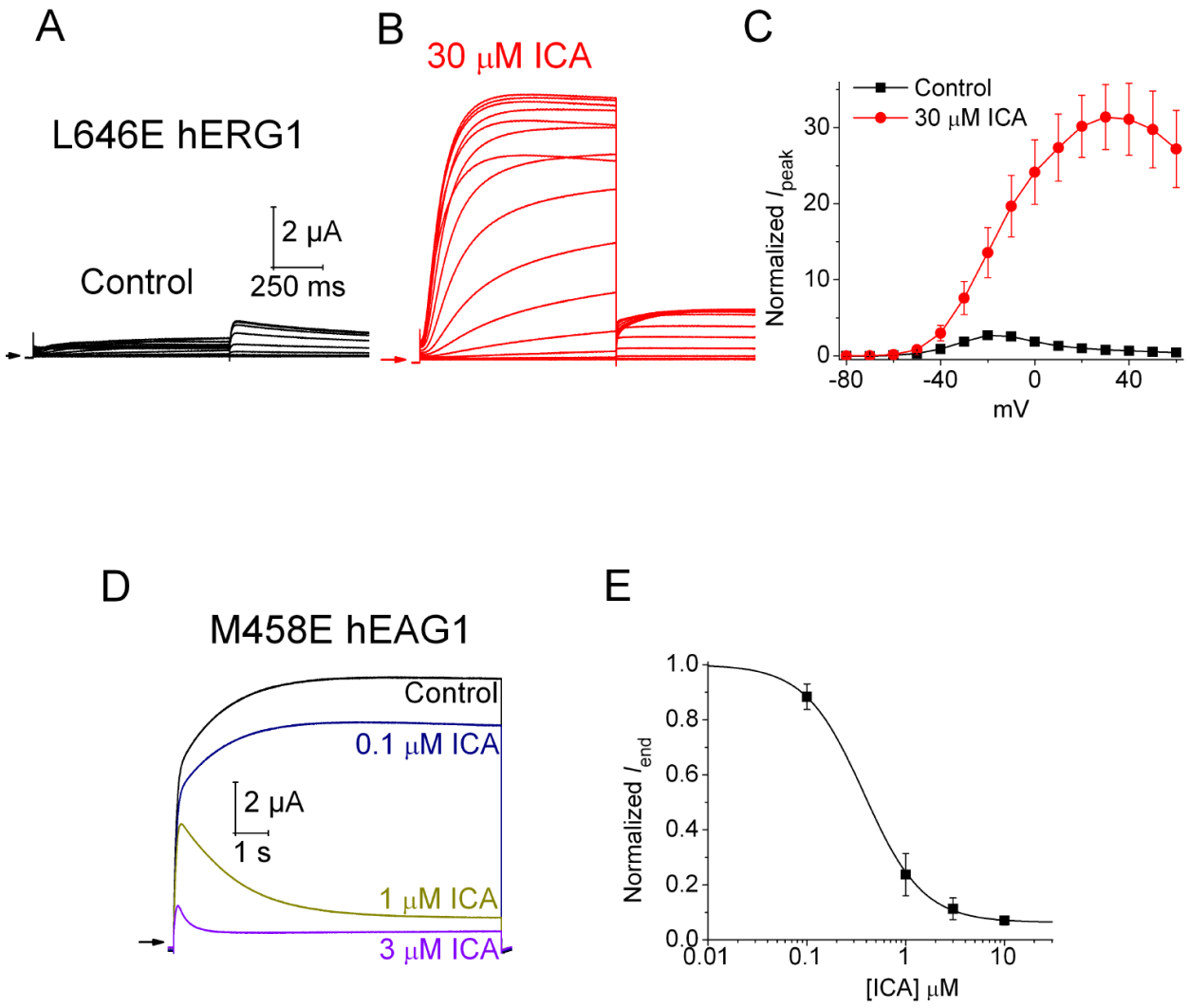


**Supplemental Fig. 4.** Effect of ICA on L646E hERG1 and M458E hEAG1 channel currents. *A* and *B*, Currents were elicited with 1-s pulses to test potentials applied in 10-mV increments from −80 to +60 mV. Tail currents were measured at −70 mV. *C*, $I_{peak}$-*V* relationships measured before (control) and in presence of 30 μM ICA ($n$ = 4). Currents were normalized relative to the peak outward control current at +20 mV. *D*, Concentration-dependent inhibition of M458E hEAG1 channel currents by ICA. Currents were elicited with 10-s pulses to +30 mV. *E*, [ICA]-response (normalized $I_{end}$ ) relationships for M458E hEAG1 channels ($IC_{50}$ = 0.45 ± 0.08 μM; $n$ = 3).

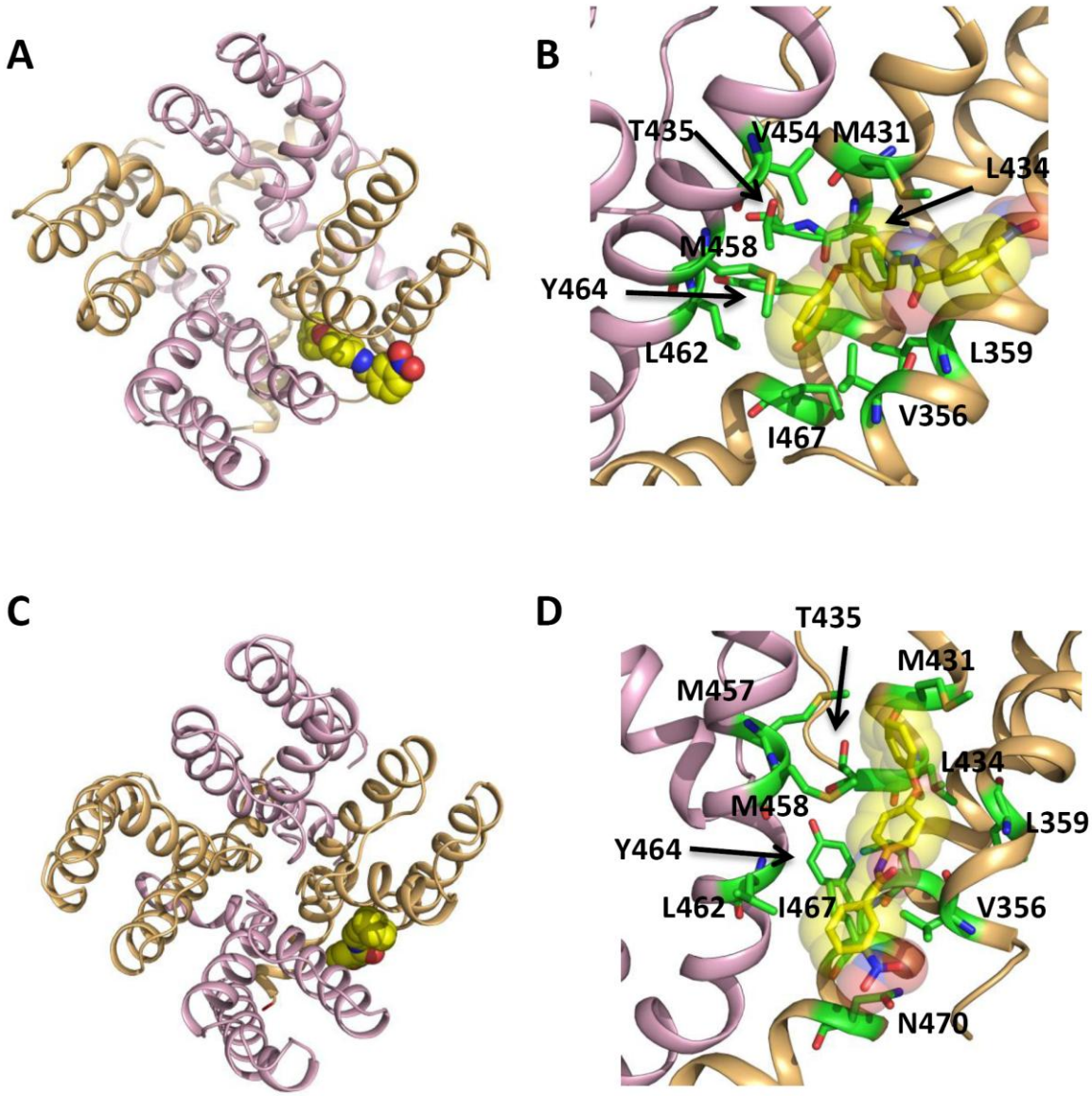


**Supplemental Fig. 5.** Molecular models of ICA docked to F359L hEAG1 channel. *A* and *B,* Extracellular view (*A*), and side-view of two adjacent subunits (*B*) with ICA bound to the open state of the F359L hEAG1 pore module. *C* and *D,* Similar views of ICA docking to closed state model.